MF/VDES R-Mode Coverage Prediction and Accuracy Estimation

Summary Report

Report No: RPT-39-JSa-20

Report Version: 1.1

Report Version Date: 14/12/2020

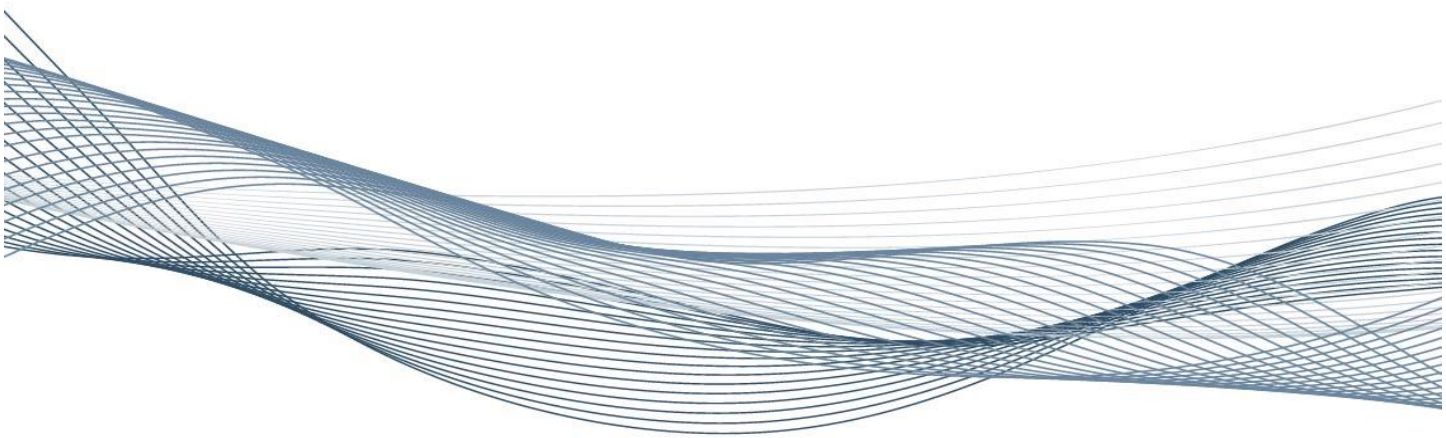

Lead Author	Reviewer	Approved for Release
Jan Šafář	Alan Grant	Martin Bransby
Research & Innovation Engineer	Principal Development Engineer	Head of Research and Development
JŠ	AG	MB

Please make comments in this box:

Report for website:

Executive Summary

The General Lighthouse Authorities' Research & Development Directorate (GRAD) was contracted by the German Federal Waterways and Shipping Administration (WSV), on behalf of the R-Mode Baltic project, to undertake VDES and combined MF/VDES R-Mode coverage and accuracy modelling.

This report provides a summary of the approach taken in the completion of these plots. The plots themselves are provided separately.

Document Disclaimer

This document is uncontrolled when removed from iManage (either electronic or printed)

Document Information

Client	M Hoppe (WSV)
Project Title	MF/VDES R-Mode Coverage Prediction and Accuracy Estimation
Deliverable/Mandate Number	I294-D1
Report Title	MF/VDES R-Mode Coverage Prediction and Accuracy Estimation – Summary Report
Report Identifier	RPT-39-JSa-20
Report Version	1.1
Report Version Date	14/12/20
Lead Author	Dr Jan Šafář
Lead Author's Contact Information	GLA Research and Development The Quay, Harwich, Essex, CO12 3JW, UK T: +44-1255-245145 E: jan.safar@gla-rad.org W: www.gla-rad.org
Contributing Author(s)	
iManage Location	
Circulation	1. Client 2. Project Files

Contents

List of Figures

List of Tables

1 Introduction

This report provides an overview of the approach and assumptions used to generate Very High Frequency (VHF) Data Exchange System (VDES) and combined VDES / Medium Frequency (MF) R-Mode coverage prediction and accuracy estimation plots and associated data, dated 1st September 2020.

This work has been completed under contract to the German Federal Waterways and Shipping Administration (WSV) as part of the R-Mode Baltic project, in a contract letter dated 30th June 2020 [1].

A list of potential R-Mode station locations to be considered under this contract was provided by WSV and reviewed by GRAD. The version used in the coverage prediction calculations is re-produced in Appendix A of this report for clarity. Plots of coverage and accuracy estimates for each station, along with their related data files, accompany this report and form the main deliverable.

2 System Configurations Considered

This study has considered the following three configurations of the R-Mode system:

1. A standalone VDES R-Mode system based on a set of existing AIS base station sites listed in Appendix A (referred to in the following as the 'VDES all-stations configuration').
2. A reduced configuration of 4 VDES R-Mode base station sites, with a focus on potential R-Mode Baltic testbed areas. Four variations of this configuration were explored.
3. A combination of the VDES all-stations configuration with supporting MF R-Mode stations listed in Appendix B.

All transmitting stations (VDES and MF) were assumed to be synchronized to within 10 ns (one-sigma) of the R-Mode reference time, in-line with assumptions made in study [2], and transmissions were assumed to be received by a combined receiver with a common clock.

It was assumed that at least 4 R-Mode stations must be simultaneously available in order for the user to be able to produce a position fix [1], [3].

Additional assumptions and parameters relevant to each of the above configurations, as well as the modelling approach taken are described in the following sections.

3 VDES R-Mode All-Stations Configuration

3.1 Geographical Area of Interest

The geographical area for the all-stations configuration was defined as follows [1], [3], [4]:

- Southern latitude: 53º N;
- Northern latitude: 60º N;
- Western longitude: 7º E;
- Eastern longitude: 20º E.

Data arrays were generated spanning the area of interest with a spatial resolution of 0.05º in both latitude and longitude, as requested by WSV and in line with study [2].

All outputs accompanying this report use the World Geodetic System 84 (WGS84) coordinate reference system.

3.2 Stations Considered

A total of 85 R-Mode stations were considered in this analysis, based on a list of existing AIS base stations located in Denmark, Germany, Poland and Sweden provided by WSV. The list was filtered

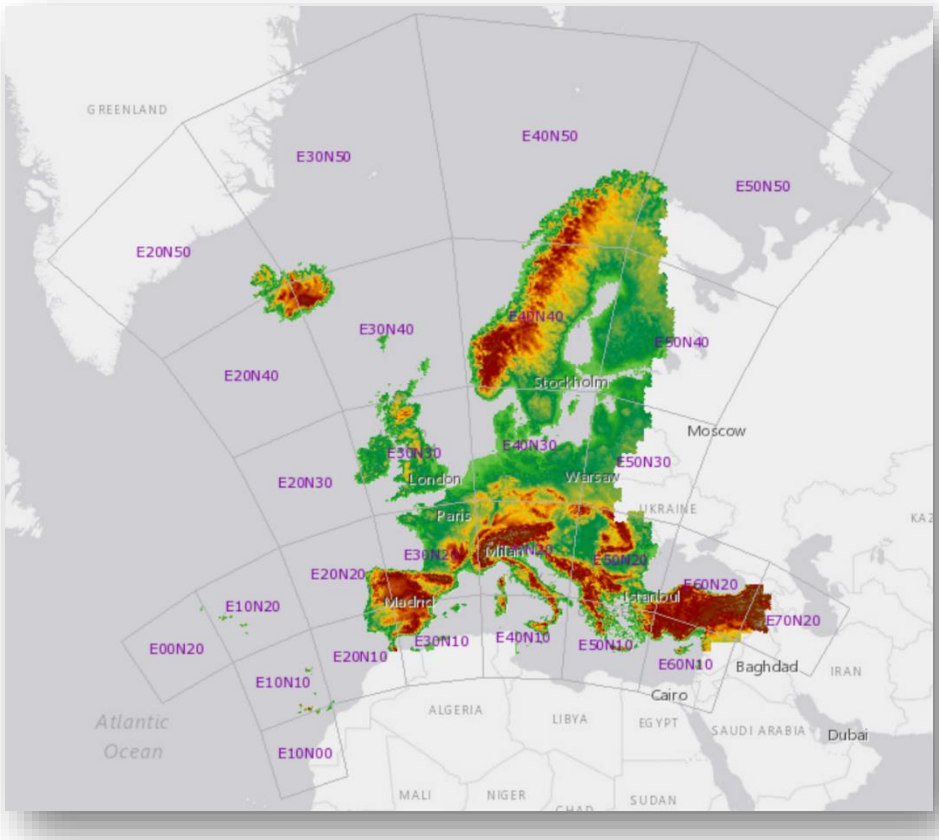

Figure 1: Geographical coverage of the terrain elevation model used.

to include stations within and up to 100 km outside of the geographical area of interest defined above. The details of the stations used, including the transmitter power, P_{TX}; transmitting antenna height, h_{TX}, antenna gain, $G_{\mathrm{TX,dBi}}$; and transmitter feeder loss, $L_{\mathrm{t,TX,dB}}$, can be found in Appendix A.

Note: Throughout this document, variables that represent quantities expressed on a logarithmic scale are denoted with the subscript dB, dBi, dBm or dBHz, as applicable.

The carrier frequency for the VDES R-Mode transmissions, f_{c}, was assumed to be 161.8375 MHz, corresponding to the centre of the upper leg of the VDE-TER 100 kHz bandwidth channel.

3.3 Received Signal Power

3.3.1 Radiowave Propagation Model

A VHF signal transmitted from a VDES R-Mode station is subject to a varying amount of attenuation, dependent on the transmitting and receiving antenna heights and separation, shape of the elevation profile along the propagation path, the climatic zone and the prevailing atmospheric conditions. In this study, the path loss incurred by the VDES R-Mode signal was modelled using a GRAD implementation of the propagation model described in Recommendation ITU-R P.2001-3 [5].

The ITU model predicts the basic transmission loss not exceeded for a given percentage of an average year. It consists of four principal sub-models to take account of different sets of propagation mechanisms:

1. Propagation close to the surface of the Earth, consisting of diffraction, non-ducting clear-air effects and precipitation fading;
2. Anomalous propagation due to ducting;
3. Propagation via atmospheric turbulence, consisting of troposcatter and precipitation fading for the troposcatter path; and
4. Propagation via the sporadic-E layer of the ionosphere.

The sub-models can be used separately or can be combined in a way that reflects the statistical correlations between the various sub-models, as described in detail in the Recommendation [5].

By examining the predicted path loss for a number of representative sea water, mixed and land paths, it was determined that, in the scenarios considered here, the contribution from the sporadic-E propagation mode (sub-model 4.) is negligible compared to the other mechanisms mentioned above and consequently only sub-models 1. to 3. were used in this study.

3.3.2 Terrain Elevation Model

The propagation model described in Rec. ITU-R P.2001 requires, as one of its inputs, a terrain profile giving heights above sea level along the great-circle radio path. Terrain elevation data for this study was obtained from the Europe-wide EU-DEM-v1.1 digital elevation model. The EU-DEM-v1.1 data is provided in tiles, each covering an area of 100 km x 100 km in size (see Figure 1). It has a horizontal resolution of 25 m and stated vertical accuracy of 7 m (RMS). For the purpose of this study, the data was transformed from the "native" ETRS89-LAEA coordinate reference system to WGS84.

3.3.3 Climatic Data

The ITU-R propagation model also requires multiple location-dependent climatic parameters to be provided, such as the expected change in refractivity in the lower layers of the atmosphere, the mean rain height, surface water-vapour density and others. For each location considered, this data was obtained by bi-linear interpolation from text files obtained from ITU-R.

3.3.4 Receiving System

The following assumptions were made with respect to the VDES R-Mode receiving system characteristics [1], [3], [6]:

- Antenna height above surface, h_{RX}: 10 m;
- Antenna type: omnidirectional, vertically polarised half-wave dipole;
- Antenna gain, $G_{\mathrm{RX,dBi}}$, : 2.15 dBi (it is assumed that a tuned antenna is used; consequently, the antenna circuit loss is considered negligible and the gain is practically equal to the antenna's directivity, $D_{\mathrm{RX,dBi}}$).
- Receiving system noise figure (including the effects of the receiver noise figure, antenna feeder loss and environmental / man-made noise emitted from sources on the vessel; for a detailed breakdown see [6]): 19 dB.

3.3.5 Data Signal Power

Similar to other radionavigation systems, R-Mode requires certain navigation data to be delivered to the receiver in order to function properly. The contents of the R-Mode navigation message has not yet been standardised but may include the surveyed coordinates of the R-Mode transmitting antennas, the health status of each station, real-time corrections and other such information. It is assumed here that the navigation data will be conveyed to the R-Mode receivers by VDES itself, using standard VDES broadcast transmissions. Therefore, in addition to the ranging functionality, the coverage model also has to consider the data communications capabilities of each VDES station used within the R-Mode system.

It is expected that, with an appropriately designed receiver, all of the three major propagation modes identified in Section 3.3.1 (i.e. diffraction, tropospheric ducting and tropospheric scattering) will contribute to the receiver's ability to successfully demodulate and decode VDES communication signals. Therefore, when modelling the received signal power for data communication purposes, sub-models 1. to 3. of Rec. ITU-R P. 2001-3 were used. The results obtained from each sub-model were combined to produce a single transmission loss figure, as described in the Recommendation [5],

The ITU model predicts the transmission loss not exceeded for a given percentage of an average year. The question then arises as to which percentile (or other statistic) of the loss should be used in coverage prediction. In this study, the decision was made to use the transmission loss not exceeded for 99.75% of the time, consistent with the 99% availability requirement for the R-Mode

system overall [7], [8] (note that given that at least four stations must simultaneously be available in any given area in order for the system to be considered available, the station availability must be at least $\sqrt[4]{0.99} \approx 0.9975$ in order for the system to meet the 99% availability requirement). Choosing a 99.75% figure provides a conservative confidence bound on the station's usable range – 99.75% of the time the range will be greater than stated. This is conservative but in keeping with the 99% system availability requirement.

The power level that can be guaranteed at the output of a loss-less receiving antenna at a distance d along a given path profile for at least 99.75% of the time can then be calculated as follows:

$$P_{\mathrm{RX,data,dBm}} = P_{\mathrm{TX,dBm}} - L_{\mathrm{t,TX,dB}} + G_{\mathrm{TX,dBi}} - L_{\mathrm{bm123,dB}}(d, h_{\mathrm{TX}}, h_{\mathrm{RX}}, \dots) + D_{\mathrm{RX,dBi}}. \quad (1)$$

In the above equation, $L_{\mathrm{bm123,dB}}$ denotes the basic transmission loss for sub-models 1. to 3. combined obtained as described above, and the remaining terms have been defined before.

For each transmitting station, the transmission loss across an area was calculated by tracing a certain number of radials from the station out to a maximum distance of 100 km and applying the ITU model along each radial. The transmission loss at points that do not lie directly on a radial was obtained by interpolation. Received power arrays were then created by applying Equation 1.

3.3.6 Ranging Signal Power

The ranging signal is a waveform with a known structure and content which is used for estimating the transmitter-receiver range (or pseudorange if the receiver and transmitter clocks are not synchronized) by measuring the time of arrival of the signal at the receiver. Our main aim when modelling this signal is to characterise the ranging accuracy that a receiver can be expected to maintain across a station's coverage area. The accuracy depends, among other things, on the received signal's carrier-power-to-noise-power-density ratio, C/N_0, and the characteristics of the multipath environment between the transmitter and the receiver.

Since the receiver estimates the great-circle distance to the transmitter, it is only those signal components propagating close to the Earth's surface that are considered useful for ranging. Signal components arriving via higher layers of the troposphere are subject to an additional propagation delay and act as a form of interference, distorting the signal time of arrival measurements. For this reason, only sub-model 1. of the ITU propagation model [5] (propagation by diffraction) was used when modelling the transmission loss and received power for the desired component of the ranging signal. Sub-models 2. and 3. (representing ducting and troposcatter) were used to model the delayed multipath signal components, as is discussed in more detail in Section 3.6.

As in the previous section, the question now arises as to what statistic of the transmission loss should be used when modelling the characteristics of the ranging signal. As will be explained in Section 3.6, in order to be able to determine the standard deviation of the ranging error required for position error calculations, the mean received power rather than the power guaranteed for a particular percentage time is required. Unfortunately, the ITU model does not provide a simple way of calculating the mean transmission loss. Therefore, the following approach was taken:

The transmission loss for sub-model 1. was considered to be a random variable, denoted here $\mathcal{L}_{\mathrm{bm1,dB}}$. A particular realisation of the random variable is denoted $L_{\mathrm{bm1,dB}}$. At each point along a given radial from the transmitter, the cumulative distribution function (CDF) of the transmission loss, denoted here $F_{\mathcal{L}_{\mathrm{bm1,dB}}}(L_{\mathrm{bm1,dB}})$, was determined by calling the ITU model multiple times for different percentage times, p, in the range from 0.00001 to 99.99999. The CDF gives the probability that the transmission loss is less than or equal to a given value:

$$F_{\mathcal{L}_{\mathrm{bm1,dB}}}(L_{\mathrm{bm1,dB}}) = \mathrm{P}(\mathcal{L}_{\mathrm{bm1,dB}} \leq L_{\mathrm{bm1,dB}}). \quad (2)$$

The quantity of interest to be determined is the mean transmission "gain" in the power domain (or the mean of the inverse of the transmission loss expressed as a ratio, $E(\mathcal{L}_{\mathrm{bm1}}^{-1})$). By realising that the expected value of a non-negative random variable $\mathcal{X}$ can be calculated from its CDF as [9]:

$$\mathrm{E}(\mathcal{X}) = \int_0^\infty 1 - F_{\mathcal{X}}(x)\,\mathrm{d}x, \tag{3}$$

noting further that the transformation between the dB loss and power gain domains is a monotonically decreasing function, and by using some fundamental properties of CDFs, the mean transmission gain (as a power ratio rather than in dB), $\mathrm{E}\left(\mathcal{L}_{\mathrm{bm1}}^{-1}\right)$, can be expressed in terms of the CDF $F_{\mathcal{L}_{\mathrm{bm1,dB}}}$ as follows:

$$\mathrm{E}\left(\frac{1}{\mathcal{L}_{\mathrm{bm1}}}\right) = \int_0^\infty F_{\mathcal{L}_{\mathrm{bm1,dB}}}(-10\log g)\,\mathrm{d}g. \tag{4}$$

The mean loss for sub-model 1. (expressed in dB) can then be defined as:

$$\bar{L}_{\mathrm{bm1,dB}} \equiv -10\log\left[E\left(\frac{1}{\mathcal{L}_{\mathrm{bm1}}}\right)\right]. \tag{5}$$

The mean loss determined using the above procedure was found to be practically identical to the median loss, as obtained from the ITU model for $p = 50$ (note, however, that is not the case for the propagation modes represented by sub-models 2. and 3., where the mean can be substantially different from the median due to the corresponding probability distributions being asymmetrical).

Transmission loss arrays were calculated by tracing a certain number of radials from each station and applying the above procedure to all points along each radial. The transmission loss at points that do not lie directly on a radial was obtained by interpolation. The mean received power arrays were then generated by applying Equation 6.

$$P_{\mathrm{RX,rng,dBm}} = P_{\mathrm{TX,dBm}} - L_{\mathrm{t,TX,dB}} + G_{\mathrm{TX,dBi}} - \bar{L}_{\mathrm{bm1,dB}}(d, h_{\mathrm{TX}}, h_{\mathrm{RX}}, \dots) + D_{\mathrm{RX,dBi}}. \tag{6}$$

3.4 Carrier-Power-to-Noise-Power-Density Ratio, C/N$_0$

The carrier-power-to-noise-power-density ratio, C/N_0, is one of the key factors that determine each station's usable range and achievable ranging accuracy. Two C/N_0 arrays were calculated for each VDES station:

$$\left(\frac{C}{N_0}\right)_{\mathrm{data,dBHz}} = P_{\mathrm{RX,data,dBm}} - N_{0,\mathrm{dBm/Hz}}$$

and

$$\left(\frac{C}{N_0}\right)_{\mathrm{rng,dBHz}} = P_{\mathrm{RX,rng,dBm}} - N_{0,\mathrm{dBm/Hz}}.$$

A noise power spectral density level of $N_{0,\mathrm{dBm/Hz}} = -155\ \mathrm{dBm/Hz}$ was assumed in line with assumptions made in reference [6], corresponding to a receiving system noise figure of $F = 19\ \mathrm{dB}$.

3.5 Station Coverage

It is assumed that an R-Mode receiver will need to be able to receive the navigation data from each VDES R-Mode station used in the position solution. In other words, each station's area of usability for ranging is assumed to be limited to its communications coverage area.

The communications coverage area for a given station was defined as the geographical area where the "data signal" carrier-power-to-noise-power-density ratio meets or exceeds the threshold required for the successful demodulation and decoding of the VDE-TER 100 kHz, Forward Error Correction (FEC)-protected, Pi/4-QPSK waveform:

$$\left(\frac{C}{N_0}\right)_{\text{data,dBHz}} \geq 55.2 \text{ dBHz}. \quad (7)$$

The C/N_0 threshold shown above was determined based on the theoretical energy-per-bit-to-noise-power-density ratio curves for the QPSK modulation and the coding gain of the VDES FEC (en)decoder for a bit error rate of 10^{-6}, as described in reference [6].

The criterion given in Equation 7 was evaluated for all points within a 100 km radius of each VDES station, and the resulting data arrays were exported in the PNG and CSV formats to the directory below:

`VDES - All Stations\Station Data\Coverage\`

3.6 Pseudorange Error

3.6.1 Error due to RF Noise and Imperfect Synchronisation

The achievable ranging accuracy in a multipath-free propagation channel with Additive White Gaussian Noise (AWGN) depends on the spectral characteristics of the ranging waveform used and the carrier-power-to-noise-power density ratio of the received signal, $(C/N_0)_{\text{rng,dBHz}}$.

Various theoretical lower bounds for the ranging accuracy can be found in the literature, such as the Cramér-Rao Bound (CRB), Modified Cramér-Rao Bound (MCRB) or the Ziv-Zakai Bound (ZZB). In this study, the ranging error was modelled using the ZZB [10], [11]. For medium-to-high C/N_0 values, the ZZB is practically identical to the MCRB, as derived for the VDE-TER R-Mode signal in reference [6], but the ZZB provides a tighter (more realistic) lower bound than the (M)CRB in the low C/N_0 region (see Figure 2). The ZZB does not have a closed-form solution and has to be evaluated numerically. The estimated standard deviation of the pseudorange error in meters obtained using the ZZB is denoted here $\sigma_{\hat{\rho},\text{ZZB}}$.

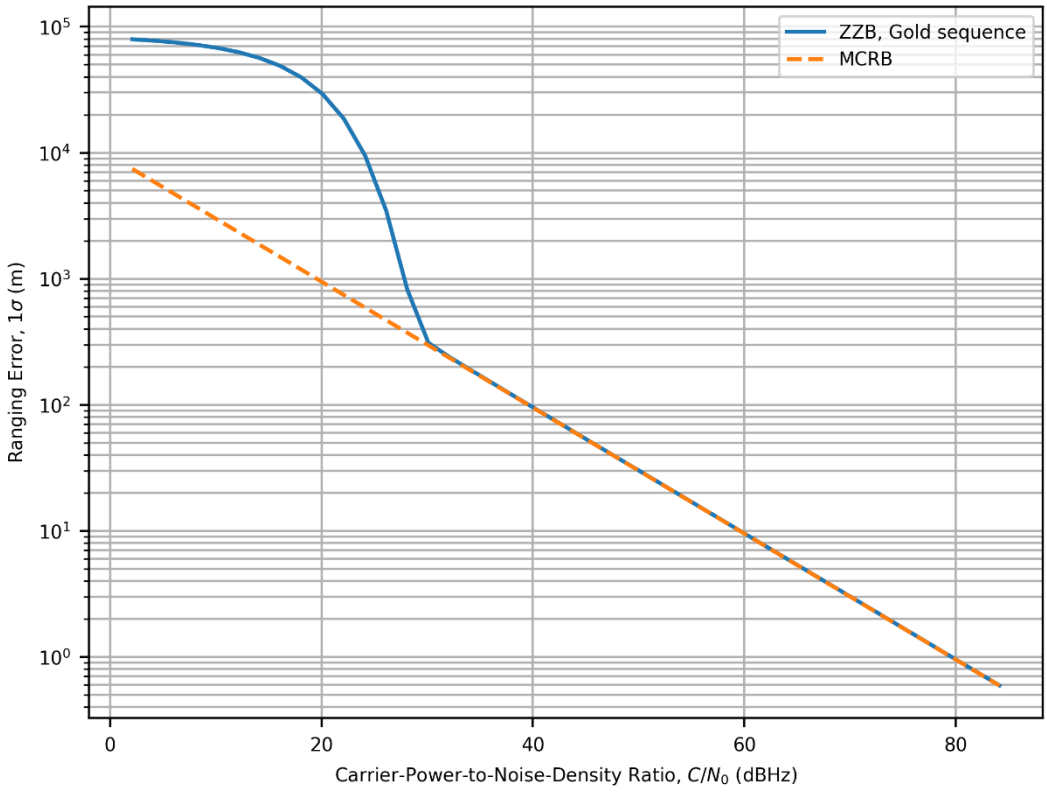

Figure 2: Performance bounds for the ranging error in a multipath-free channel with AWGN.

The ranging waveform assumed in the ZZB calculations consisted of a Gold-code sequence of length 1877 symbols, modulated onto a VDE-TER carrier with a rate or 76,800 symbols per second using the Pi/4-QPSK modulation; further details of the waveform can be found in reference [12].

In line with study [2], a constant term, $\sigma_{\hat{\rho},\mathrm{TX}} \approx 3\ \mathrm{m}$, was added to the pseudorange error budget, representing achievable transmitter synchronisation accuracy of $10\ \mathrm{ns}$ (one-sigma):

$$\sigma_{\hat{\rho},\mathrm{noise}} = \sqrt{\sigma^2_{\hat{\rho},\mathrm{ZZB}} + \sigma^2_{\hat{\rho},\mathrm{TX}}}. \tag{8}$$

Equation 8 was evaluated for all points within a 100 km radius of each VDES station, and the resulting data arrays were exported in the PNG and CSV formats to the directory below:

`VDES - All Stations\Station Data\Ranging Error – Noise\`

3.6.2 Error due to Multipath Propagation

As explained in Section 3.3.1 and Section 3.3.5, there are three principal modes that contribute to VHF signal propagation over the distances considered in this study: diffraction, tropospheric ducting and tropospheric scattering. Only the first mode (diffraction) is considered useful for ranging; the remaining two constitute a form of multipath interference. In order to provide an indication of the magnitude of pseudorange error likely to be experienced due to multipath, a simple semi-analytic model was developed as described below.

The complex envelope of the received signal, $r(t)$, was modelled as a sum of a wanted component (representing the diffraction mode) and an unwanted component, representing the signal energy reaching the receiver through ducting and troposcatter:

$$r(t) = s(t) + \underbrace{\frac{1}{\sqrt{R_{\mathrm{S/I}}}} s(t-\tau) e^{-i2\pi f_c \tau}}_{\text{interference}}. \tag{9}$$

In the above equation, $s(t)$ is the complex envelope of the ranging waveform (defined in Section 3.6.1), $R_{\mathrm{S/I}}$ is the assumed signal-power-to-interference-power ratio (SIR), τ is the assumed delay of the unwanted component with respect to the wanted signal and $f_c = 161.8375\ \mathrm{MHz}$ is the carrier frequency of the ranging signal. The complex exponential term in the interference expression represents the carrier phase shift due to the delay, τ.

A receiver measures the time of arrival of the R-Mode signal (and hence the pseudorange) by correlating the received signal, $r(t)$, with a replica of the transmitted waveform, $s(t)$. By evaluating the correlation for a range of lags, it is possible to visualise the distortion to the correlation peak caused by the multipath interference and assess the attendant error in the time-of-arrival measurement. This is illustrated in Figure 3 which shows the magnitude of the normalised cross-correlation between the received signal and the ranging waveform replica, zooming in on the main correlation peak. The upper part of Figure 3 shows the ideal shape of the correlation peak in the absence of any multipath components. The bottom part of the figure then shows the result of adding a multipath component with a power 10 dB below that of the wanted signal, delayed by 10 µs. The resulting distortion to the correlation peak depends very much on the carrier phase difference between the wanted and unwanted components. In the case shown here, the distortion happens to be such that the position of the peak is shifted by approximately 1 µs to the left, introducing a pseudorange error of approximately 300 m.

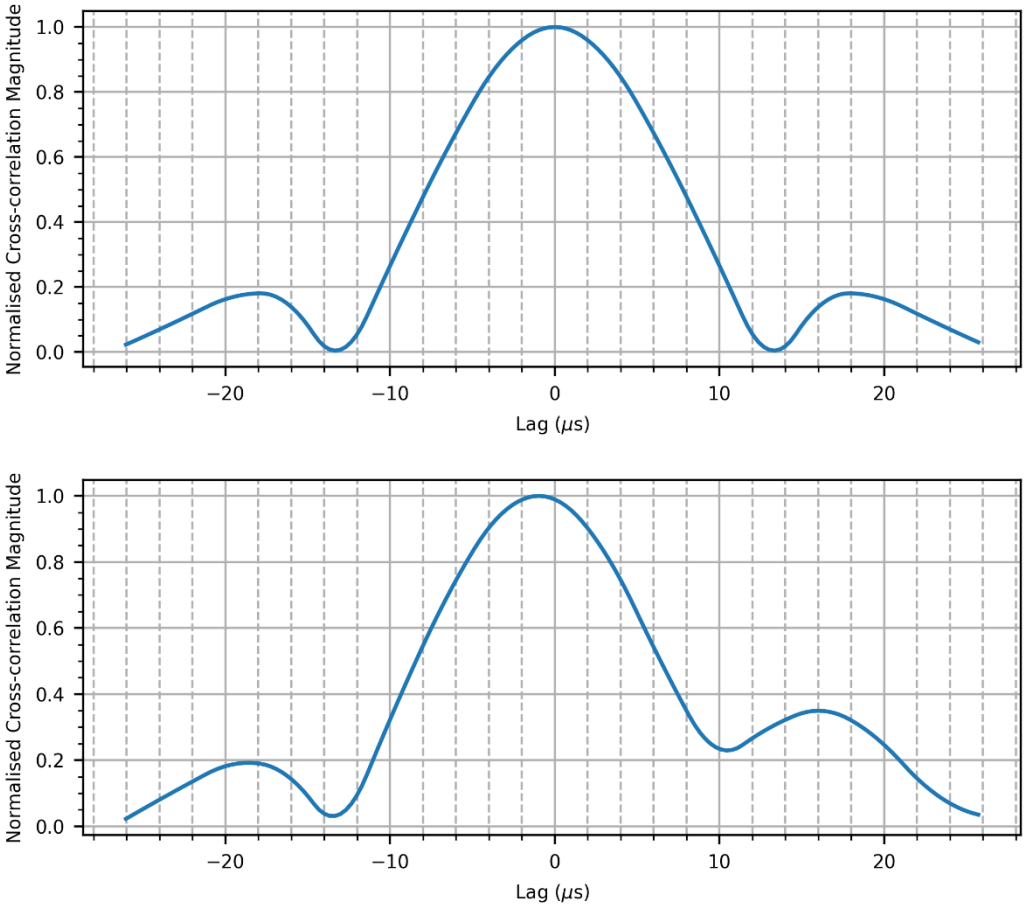

Figure 3: Shape of the correlation peak for a multipath-free signal (top) and a signal affected by multipath with a SIR of 10 dB and a delay of 10 μs (bottom).

The excess delay of the multipath component(s), τ, is a function of the transmitter-to-receiver separation, d, and the effective altitude of the duct or the area of the troposphere where the scattering takes place, h_{tropo}, Assuming a simple geometrical model, the delay can be expressed as follows:

$$\tau = \frac{\sqrt{4h_{\text{tropo}}^2 + d^2} - d}{c}, \tag{10}$$

where c is the speed of light in free space.

The height of the troposcatter common volume can be estimated using the ITU propagation model [5] and is typically found to be less than about 500 m in the area of interest. Reference [13] suggests that, at mid-latitudes, the duct altitude does not exceed 1900 m, with the number of ducts observed decreasing with increasing altitude. Therefore, the effective altitude, h_{tropo}, was modelled here as a realisation of a random variable, $\mathcal{H}_{\text{tropo}}$, with a triangular distribution, with the lower limit and mode of 0 m and the upper limit of 1900 m. Under these assumptions, the excess delay is always less than around 13 μs, i.e. less than the duration of a single symbol at the highest VDE-TER symbol rate.

Numerical simulations were performed incorporating the above models and assumptions. 100,000 values of h_{tropo} were drawn from the triangular distribution and Equation 10 was used to calculate the corresponding excess delay, τ, at a number of points up to a distance of 100 km from the

transmitter. The excess delay, τ, can therefore be viewed as a realisation of a random variable, denoted here $\mathcal{T}$.

At each geographical point, the received signal $r(t)$ was generated for each value of τ, and a range of SIR values between 0 dB and 40 dB and each of these signal realisations were correlated with the ranging waveform, $s(t)$. The difference between the time corresponding to the peak of the correlation function and the actual time of arrival of the ranging signal $s(t)$ was then used to determine the instantaneous pseudorange error, $\varepsilon_{\hat{\rho}}$.

Since the excess delay is considered a realisation of a random variable $\mathcal{T}$, also the pseudorange error at a particular distance from transmitter, d, and for a particular SIR, $R_{S/I}$, becomes a random variable: $\mathcal{E}_{\hat{\rho}}(\mathcal{T}; R_{S/I}, d)$. The RMS pseudorange error as a function of the SIR and distance was calculated as follows[1],

$$\sqrt{P(R_{S/I}, d)} \equiv \sqrt{\mathrm{E}\left[\mathcal{E}_{\hat{\rho}}^2(\mathcal{T}; R_{S/I}, d)\right]},$$

and is plotted in Figure 4. A similar plot can be obtained for the bias in the pseudorange measurement caused by the multipath interference,

$$b \equiv \mathrm{E}\left[\mathcal{E}_{\hat{\rho}}(\mathcal{T}; R_{S/I}, d)\right].$$

As could be expected, the effects of multipath interference fade away with increasing SIR and distance from the transmitter. The latter is a consequence of the excess delay spread approaching zero with $d \to \infty$, as can be seen from Equation 10.

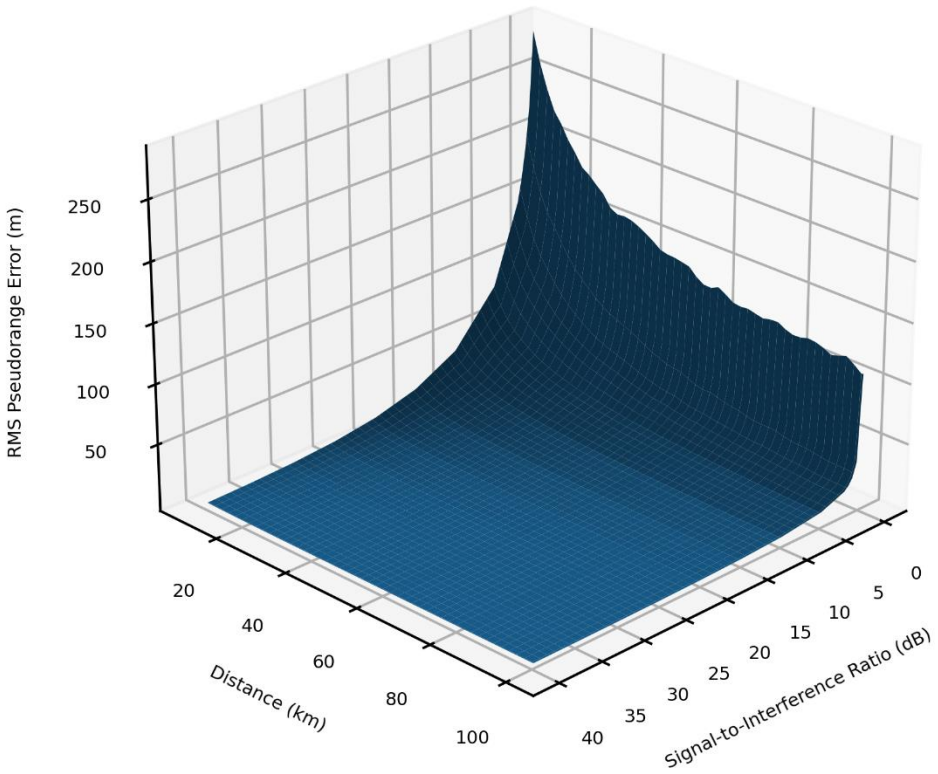

Figure 4: RMS ranging error due to multipath propagation as a function of the transmitter-receiver separation and SIR.

[1] $\mathrm{E}[\cdot]$ denotes the statistical expectation operator.

Note: Figure 4 is the result of numerical simulations and shows what the ranging error would be if an R-Mode signal was received at a given distance from the transmitter (corresponding to a certain distribution of excess delay) at a given SIR. The figure does not consider the probability of a particular SIR actually being observed at the given distance. This information is introduced to the model at the next step which involves detailed path profile analysis and transmission loss modelling. Please note that the probability of a low SIR occurring at a short distance is relatively small, which means that the extreme errors seen in Figure 4 are relatively unlikely to occur in reality.

The last step is to connect the above results to the statistics of the transmission loss for the three dominant propagation modes available from the ITU propagation model [5]. This can be done by modelling the SIR as a realisation of a random variable, $\mathcal{R}_{S/I}$, whose statistical properties are derived from the ITU propagation model.

Note: In the derivation of the following results, the wanted signal power (which appears in the numerator of the SIR) was approximated by its mean value. This is considered to be a justifiable simplification as the power of the wanted signal, represented by sub-model 1 of the ITU model, shows significantly less variability than the power of the unwanted components (i.e. the denominator of the SIR), represented by sub-models 2. and 3.

If both the SIR and delay are considered random variables as described above, then the following expressions can be derived for the mean and standard deviation of the pseudorange error, respectively:

$$\mu_{\hat{\rho},\mathrm{mult}} = \sqrt{\int_0^\infty F_{\mathcal{L}_{\mathrm{bm23,dB}}}\left[\alpha^{-1}(b;d) + \bar{L}_{\mathrm{bm1,dB}}\right] db},$$

$$\sigma_{\hat{\rho},\mathrm{mult}} = \sqrt{\int_0^\infty F_{\mathcal{L}_{\mathrm{bm23,dB}}}\left[\beta^{-1}\left(\sqrt{P};d\right) + \bar{L}_{\mathrm{bm1,dB}}\right] dP - \mu_{\varepsilon_{\hat{\rho}}}^2},$$

where:

$F_{\mathcal{L}_{\mathrm{bm23,dB}}}$ is the CDF of the transmission loss for the unwanted signal components obtained by evaluating the transmission loss for sub-models 2. and 3. of the ITU propagation model [5] over a range of time-percentages, p, and combining the results for each value of p as described in Recommendation [5]; and

α^{-1} and β^{-1} are functions that map a given pseudorange bias, b, and RMS pseudorange error, $\sqrt{P}$, respectively, to the corresponding SIR at a particular distance from transmitter, d; for a given d, these functions were obtained by inverting the bias vs. SIR and RMS ranging error vs. SIR functions, respectively, obtained by numerical simulations (see Figure 4).

The mean pseudorange error (or pseudorange bias), $\mu_{\varepsilon_{\hat{\rho}}}$, is typically much smaller than the standard deviation, $\sigma_{\varepsilon_{\hat{\rho}}}$, and therefore its impact on the position solution will not be considered further in this study.

3.6.3 Combined Error

The combined ranging error due to RF noise, imperfect transmitter synchronisation and multipath propagation is given by the following expression:

$$\sigma_{\hat{\rho}} = \sqrt{\sigma_{\hat{\rho},\mathrm{noise}}^2 + \sigma_{\hat{\rho},\mathrm{mult}}^2}. \qquad (11)$$

Equation 11 was evaluated for all points within a 100 km radius of each VDES station, and the resulting data arrays were exported in the PNG and CSV formats to the directory below:

VDES - All Stations\Station Data\Ranging Error – Combined

Sample plots for both the ranging error due to noise/synchronization and the combined error are provided in Section 3.8.

3.7 Position Solution

It is assumed that the positioning processor will form a Weighted Least Squares (WLS) solution of an over-determined system of pseudorange measurements, as described in study [2].

Figure 5 shows the number of VDES stations available over the area of interest. In this study, four stations are considered to be the minimum number required in order to produce a position fix. The area where at least four stations are expected to be available is shown in Figure 6.

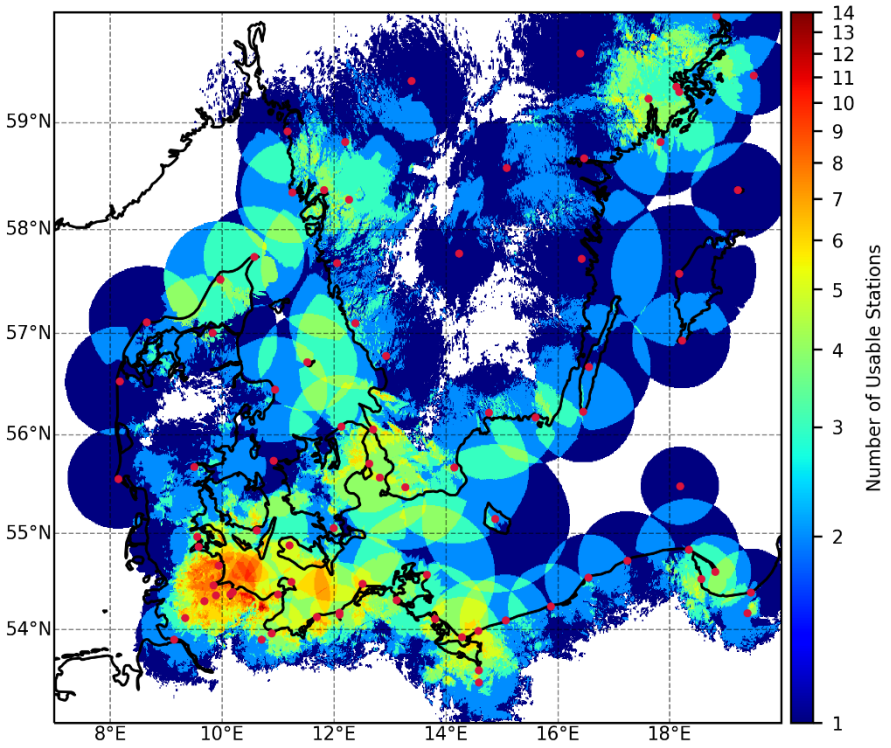

Figure 5: Number of available VDES stations for a target station availability of 99.75%.

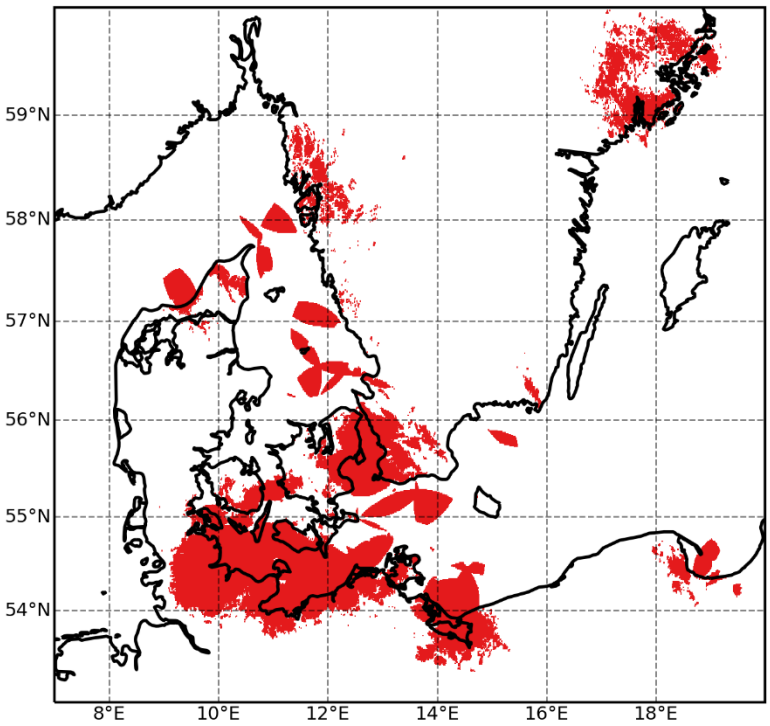

Figure 6: System coverage area for a minimum of 4 available stations and a target system availability of 99%.

The accuracy of the position solution achievable within the predicted coverage area was determined using the Harre approximation [14] which provides an estimate of the horizontal position error not exceed with a probability of 95% (R95):

$$a_{\mathrm{R95}} \approx (1.960787 + 0.004121 \cdot c + 0.114151 \cdot c^2 + 0.371707 \cdot c^3) \cdot \sigma_{\mathrm{ma}}. \qquad (12)$$

In the above equation, $c = \sigma_{\mathrm{mi}}/\sigma_{\mathrm{ma}}$, with σ_{mi} and σ_{ma} being the semi-minor and semi-major axis, respectively, of the one-sigma iso-probability ellipse calculated as described in study [2]. Numerical simulations show that the Harre approximation provides a more accurate estimate of the true 95$^{\mathrm{th}}$-percentile error for a wide range of transmitter-receiver geometries than the Rayleigh distribution approach used in study [2], or the commonly-used approach based on scaling the DRMS[2] position error.

Two position accuracy plots were produced for the VDES all stations configuration – one based on the "noise-only" pseudorange error data, $\sigma_{\hat{\rho},\mathrm{noise}}$, representing the achievable positioning accuracy in an idealised, multipath-free propagation channel, and one based on the combined error data, $\sigma_{\hat{\rho}}$, which represents the first attempt at modelling the effects of multipath propagation on VDES R-Mode accuracy. The results are shown in Figure 7 and Figure 8, respectively.

The system coverage and positioning error data arrays were exported in the PNG and CSV formats to the directory below:

`VDES - All Stations\Combined Data Sets\`

[2] Distance Root-Mean-Squared

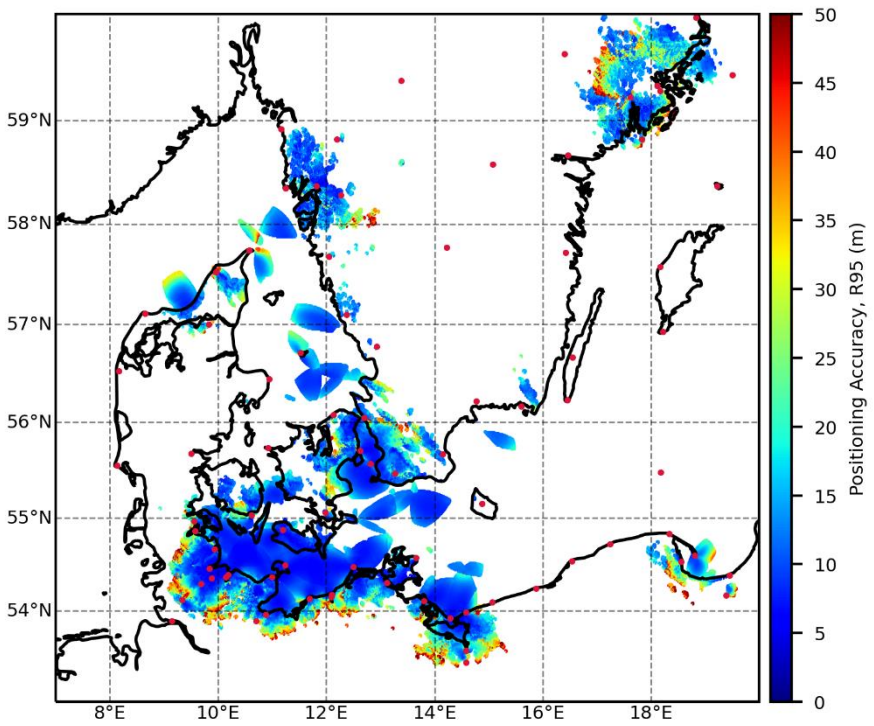

Figure 7: Predicted positioning accuracy for the VDES all stations configuration, assuming a multipath-free propagation channel.

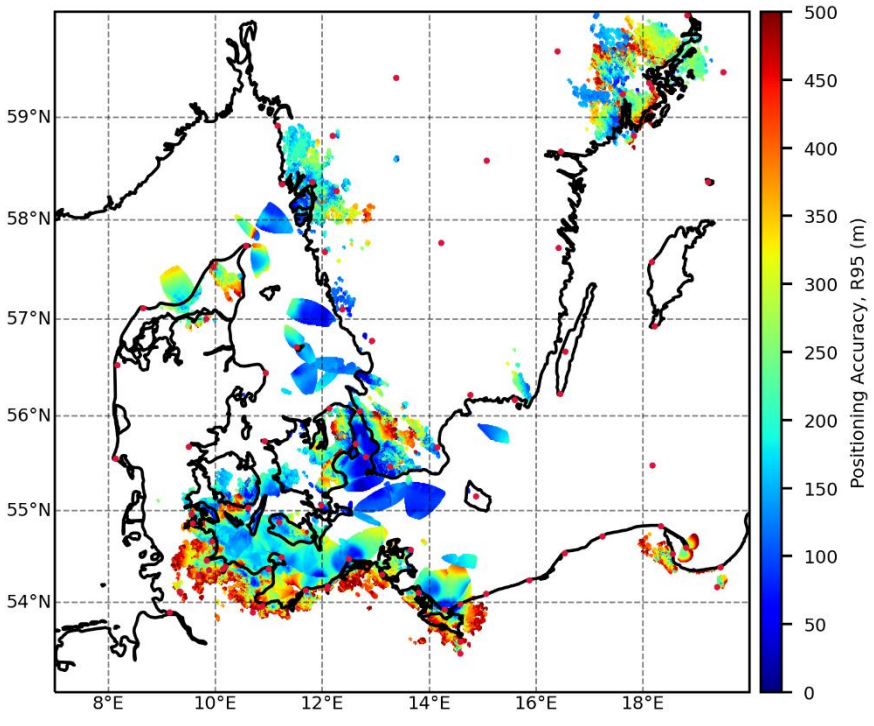

Figure 8: Predicted positioning accuracy for the VDES all stations configuration, including the effects of multipath propagation (note: the multipath model used has yet to be fully validated).

3.8 Traceability

The coverage and performance model used was validated against data collected during the VDES R-Mode measurement campaign conducted by the National Institute of Telecommunications (NIT), Poland, on behalf of the R-Mode Baltic project in November 2019 [12]. During the campaign, R-Mode signals were transmitted from a tower located at the premises of the Maritime Office in Gdynia and received on-board a ferry operating on a route between Gdynia, Poland and Karlskrona, Sweden. The transmitter and receiver antenna heights were 28 m and 25 m above sea level, respectively (note that the latter is significantly higher than the height assumed in the rest of this study which has a noticeable impact on the achievable coverage and performance); the transmitter power was 50 W. For further details of the measurement setup see reference [12].

Figure 9 shows the predicted ranging error due to RF noise and imperfect transmitter synchronisation, $\sigma_{\hat{\rho},\mathrm{noise}}$, for the NIT station, plotted up to the 30 m contour. While the level of performance indicated appears to be achievable in numerical simulations using a line-of-sight, multipath-free channel model, the ranging errors observed during the sea trials were approximately an order of magnitude higher than the predictions, as can be seen in Figure 10. It seems likely that the discrepancy between the predicted and observed ranging error is largely due to the effects of multipath propagation but other factors, such as propagation delay biases due to elevated terrain, various implementation losses and equipment imperfections may have had a significant impact as well.

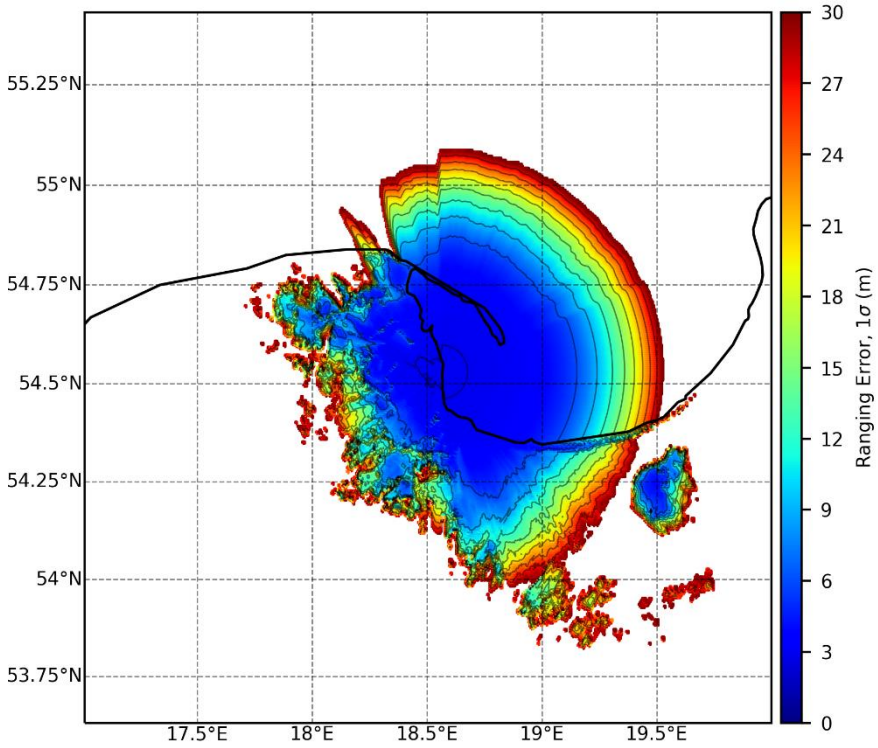

Figure 9: Predicted ranging error due to RF noise and imperfect transmitter synchronisation for the NIT station.

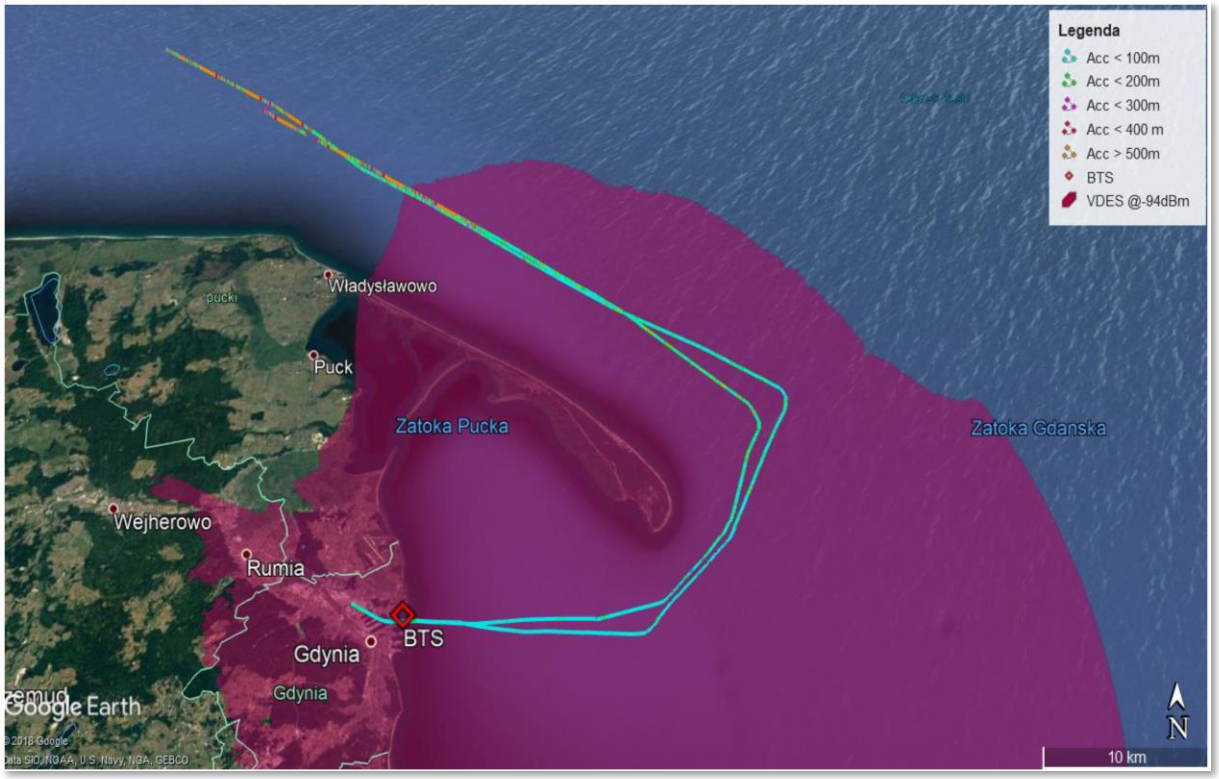

Figure 10: Ranging error for the NIT station observed during VDES R-Mode trials conducted by the R-Mode Baltic project in November 2019.

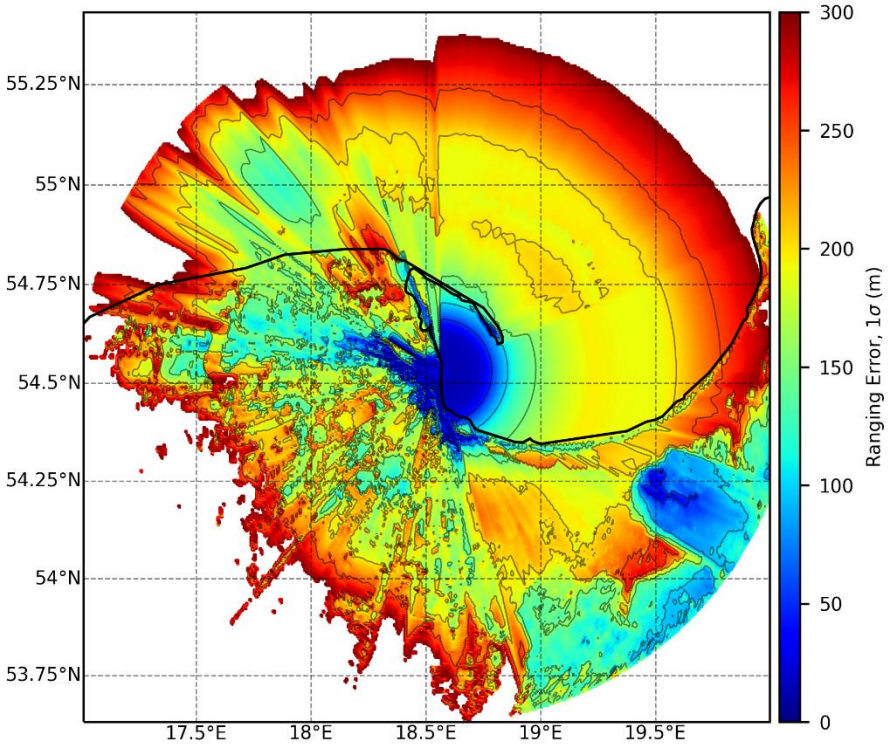

Figure 11: Predicted ranging error due to RF noise, imperfect synchronisation and multipath propagation for the NIT station.

Figure 11 shows the predicted combined ranging error, $\sigma_{\hat{\rho}}$, which includes the modelled effects of multipath interference. This plot appears to be in a very good agreement with the experimental results shown in Figure 10. The ranging error is predicted to be less than 50 m across much of the area between the coastline and the Hel Peninsula; it reaches 100 m at the tip of the peninsula; is in the 100-200 m region in the area immediately north of the peninsula and exceeds 200 m in the area north-west of Hel, which is in the shadow of some elevated terrain.

Finally, Figure 12 shows the predicted coverage area for the NIT station. As explained in Section 3.5, this represents the area of reliable VDE-TER data reception. A comparison of Figure 12 with Figure 10 shows that, as expected, it is possible to derive pseudorange measurements from the VDES R-Mode signal outside the communications coverage area of a VDES station. However, the assumption here is that the positioning processor will need to receive the navigation data from each station used in the position solution and therefore, for the purpose of this study, each VDES station's area of usability was limited to its communications coverage area.

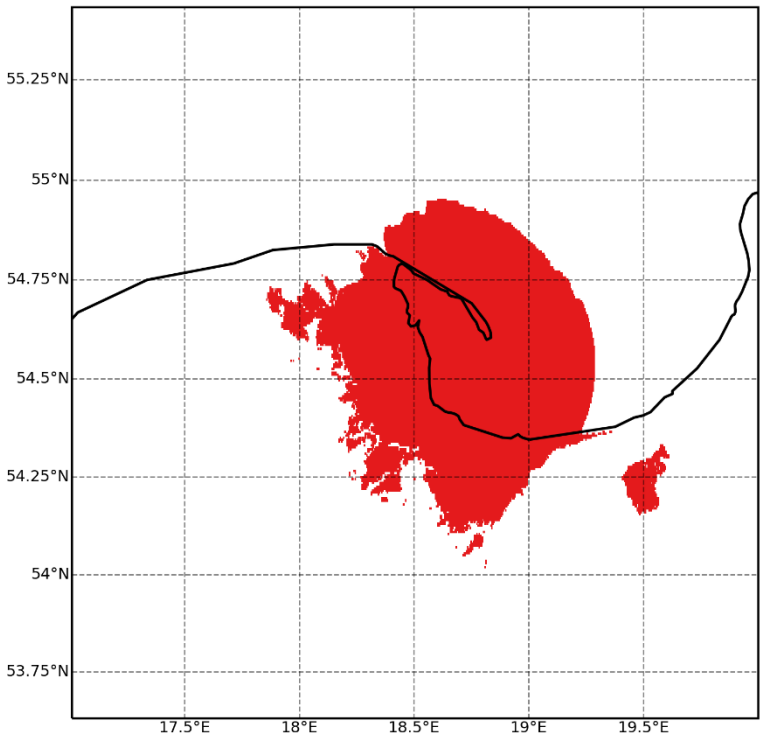

Figure 12: Predicted coverage area for the NIT station.

4 VDES R-Mode Reduced Configurations

4.1 Testbed Areas

Four geographical areas were identified by WSV for closer examination, as shown in Figure 13 and detailed in the following sections.

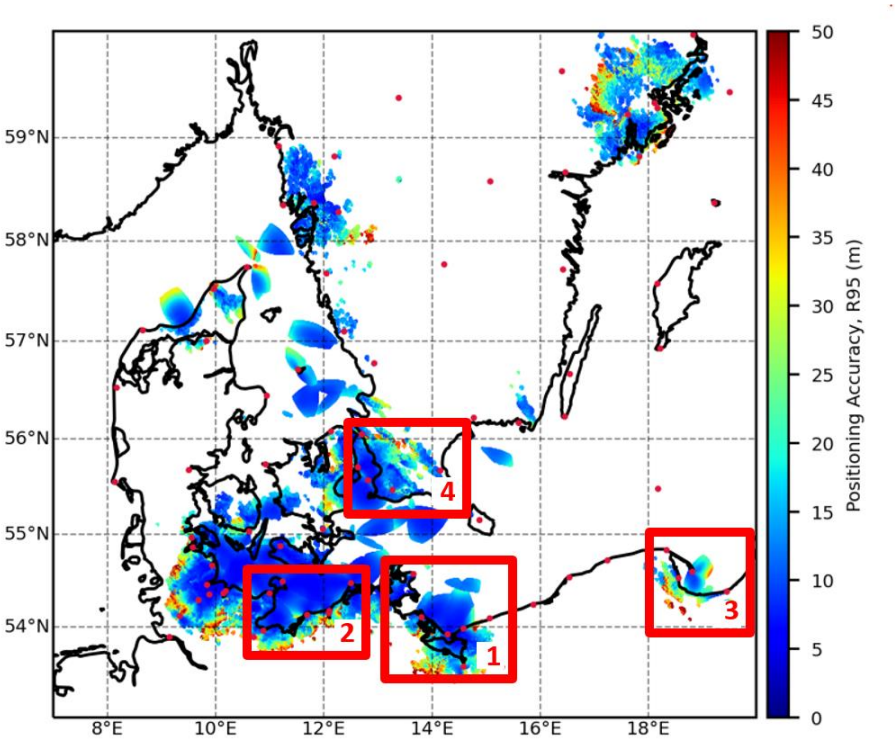

Figure 13: Testbed areas considered.

4.2 Testbed 1

4.2.1 Geographical Area of Interest

The first testbed area lies on the border between Germany and Poland and is bounded as follows:

- Southern latitude: 53.5° N;
- Northern latitude: 54.8° N;
- Western longitude: 13° E;
- Eastern longitude: 15.5° E.

4.2.2 Stations Considered

The following VDES stations were selected by WSV for inclusion in Testbed 1 (details of the stations can be found in Appendix A):

- Stubbenkammer;
- Karlshagen;
- Swinoujscie;
- Kikut.

4.2.3 Results

The individual station and system-level data arrays for this configuration were exported in the PNG and CSV formats to the directory below:

VDES – Testbed 1

Sample results are provided here in Figure 14 and Figure 15.

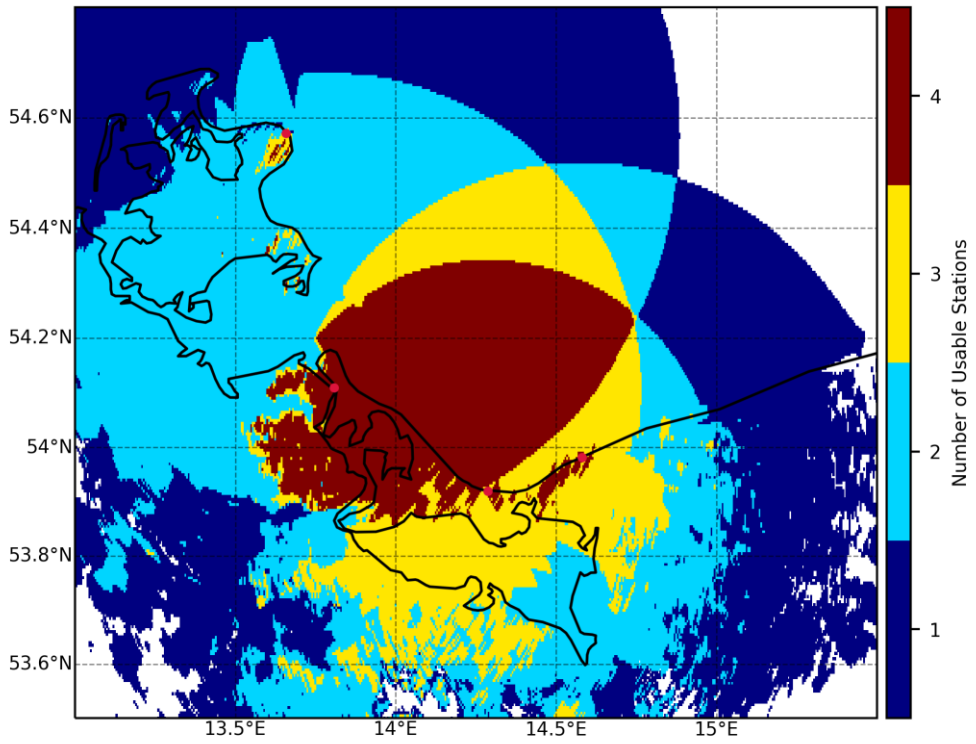

Figure 14: Number of available VDES stations for Testbed 1; target station availability: 99.75%.

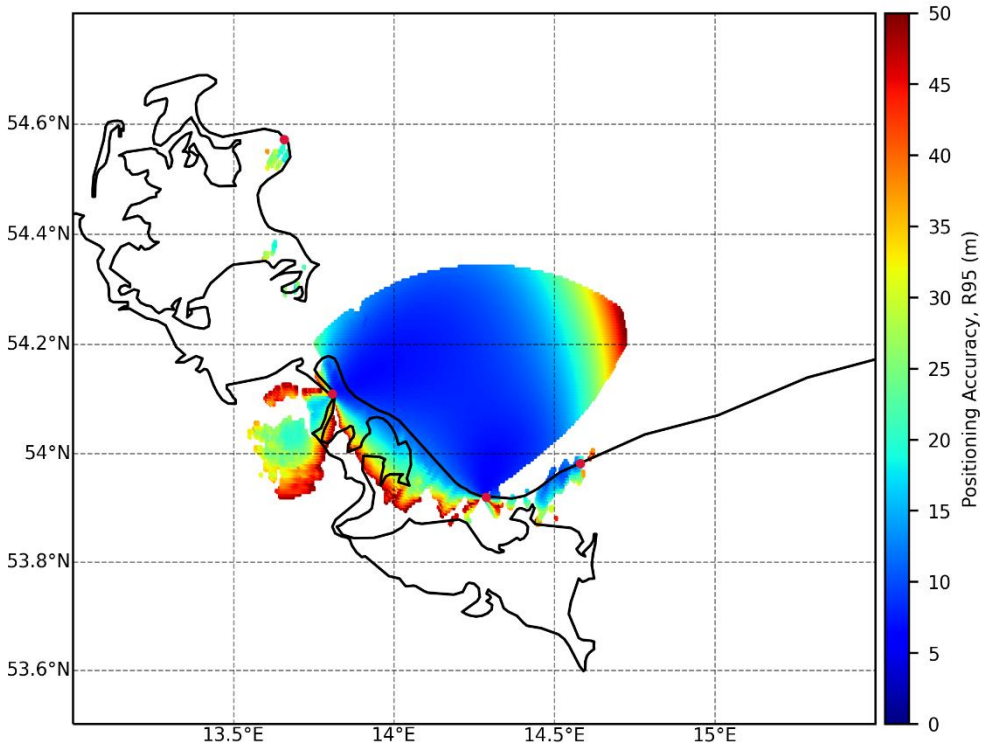

Figure 15: Predicted positioning accuracy for Testbed 1, assuming a multipath-free propagation channel.

4.3 Testbed 2

4.3.1 Geographical Area of Interest

The second testbed area lies off the coast of Germany and is bounded as follows:

- Southern latitude: 53.7° N;
- Northern latitude: 54.7° N;
- Western longitude: 10.5° E;
- Eastern longitude: 12.8° E.

4.3.2 Stations Considered

The following VDES stations were selected by WSV for inclusion in Testbed 2 (for details see Appendix A):

- Darßer Ort;
- Warnemünde;
- Buk;
- Marienleuchte.

4.3.3 Results

The results for this configuration can be found in the directory below:

`VDES – Testbed 2\`

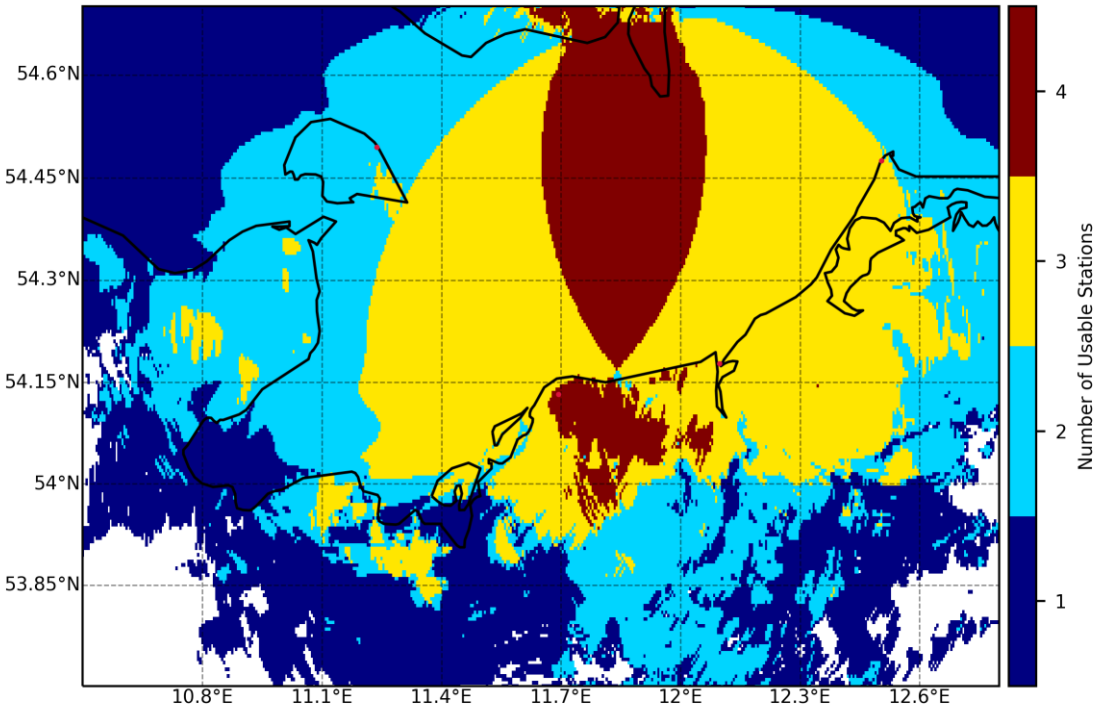

Figure 16: Number of available VDES stations for Testbed 2; target station availability: 99.75%.

4.4 Testbed 3

4.4.1 Geographical Area of Interest

The third testbed area lies off the coast of Poland and is bounded as follows:

- Southern latitude: 54.0° N;
- Northern latitude: 55.0° N;
- Western longitude: 18.0° E;

- Eastern longitude: 20.0º E.

4.4.2 Stations Considered

The following VDES stations were selected by WSV for inclusion in Testbed 3 (for details see Appendix A):

- Rozewie;
- Hel;
- RL Gdynia;
- Krynica Morska.

4.4.3 Results

The results for this configuration can be found in the directory below:

`VDES – Testbed 3\`

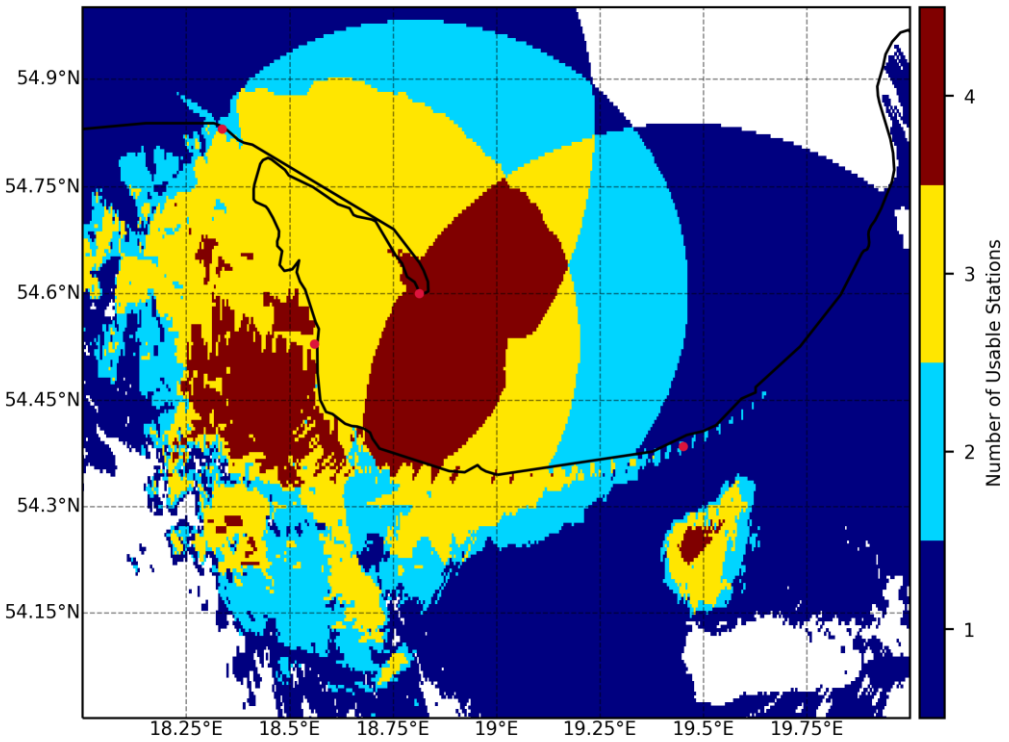

Figure 17: Number of available VDES stations for Testbed 3; target station availability: 99.75%.

4.5 Testbed 4

4.5.1 Geographical Area of Interest

The fourth testbed area stretches across the southern tip of the Scandinavian Peninsula and is bounded as follows:

- Southern latitude: 55.2º N;
- Northern latitude: 56.2º N;
- Western longitude: 12.4º E;
- Eastern longitude: 14.8º E.

4.5.2 Stations Considered

The following VDES stations were selected by WSV for inclusion in Testbed 4 (for details see Appendix A):

- Helsinborg;
- Öresundsbron;
- Trelleborg;
- Lynetten.

4.5.3 Results

The results for this configuration can be found in the directory below:

`VDES – Testbed 4\`

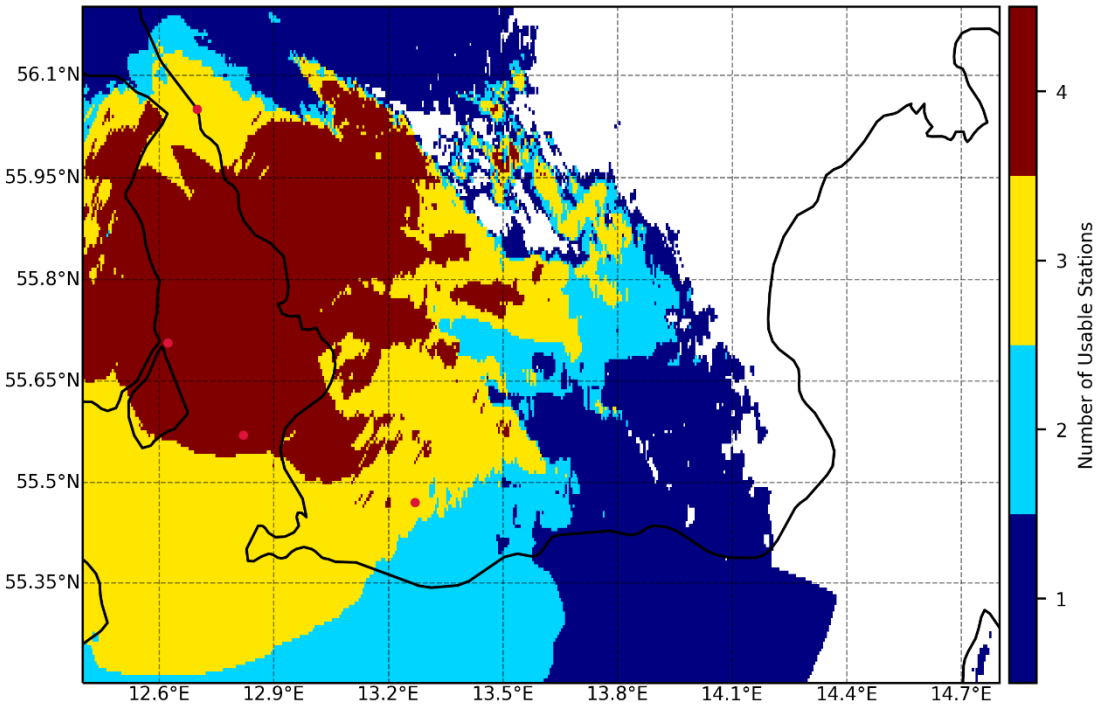

Figure 18: Number of available VDES stations for Testbed 4; target station availability: 99.75%.

5 Combined MF/VDES R-Mode Configuration

5.1 Geographical Area of Interest

The target geographical area for this analysis was identical to that used for the VDES all-stations configuration.

5.2 Stations Considered

85 VDES stations and 8 supporting MF stations were included in this analysis, as detailed in Appendix A and Appendix B, respectively.

5.3 Station Coverage

5.3.1 VDES Stations

Identical VDES station coverage criteria were used as in the preceding analyses presented in this report (for details see Section 3.5).

5.3.2 MF Stations

In line with study [2], the coverage area of an MF station was defined as the geographical area where the predicted daytime pseudorange error does not exceed 10 m (one sigma) and the sky-

wave-induced pseudorange error does not exceed 200 m (one sigma). Two separate datasets were produced representing the daytime and night-time conditions, respectively.

Please note that the MF coverage criteria used do not guarantee successful reception of the data carried by the MF signal.

5.4 Pseudorange Error

5.4.1 VDES Stations

Identical VDES pseudorange error models were used as in the preceding analyses presented in this report (for details see Section 3.6).

5.4.2 MF Stations

MF pseudorange error data generated in study [2] was used; no new modelling was performed.

5.5 Position Solution

Since all R-Mode stations used in this analysis were assumed to be accurately synchronized with each other and transmissions were assumed to be received by a combined receiver with a common clock (see Section 2), there was no need to consider any inter-system timing biases (MF vs. VDES) and the same approach could be used to model the accuracy of the combined MF/VDES position solution as was used for standalone VDES R-Mode positioning (see Section 3.7).

The system coverage and positioning error data arrays were exported in the PNG and CSV formats to the directory below:

`VDES and MF\`

Data for daytime and night-time conditions were placed in separate sub-directories.

Individual station data was not included in this case as this had been provided as part of the VDES all-station configuration and the MF study [2].

Sample plots are presented below.

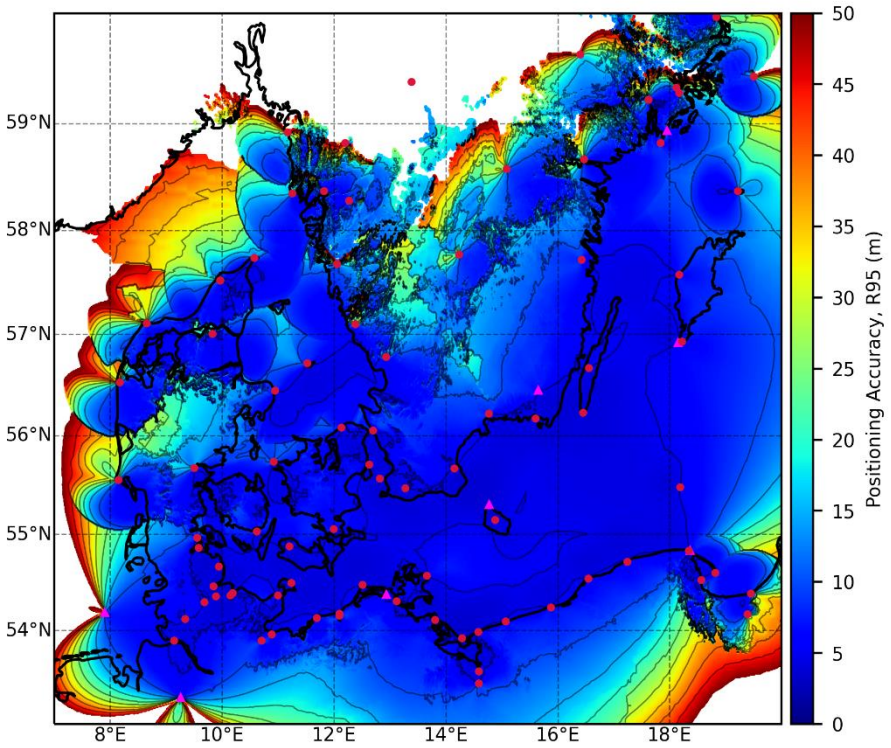

Figure 19: Predicted daytime positioning accuracy for the combined MF/VDES configuration, assuming a multipath-free VDES propagation channel; red dots – VDES stations; magenta triangles – MF stations.

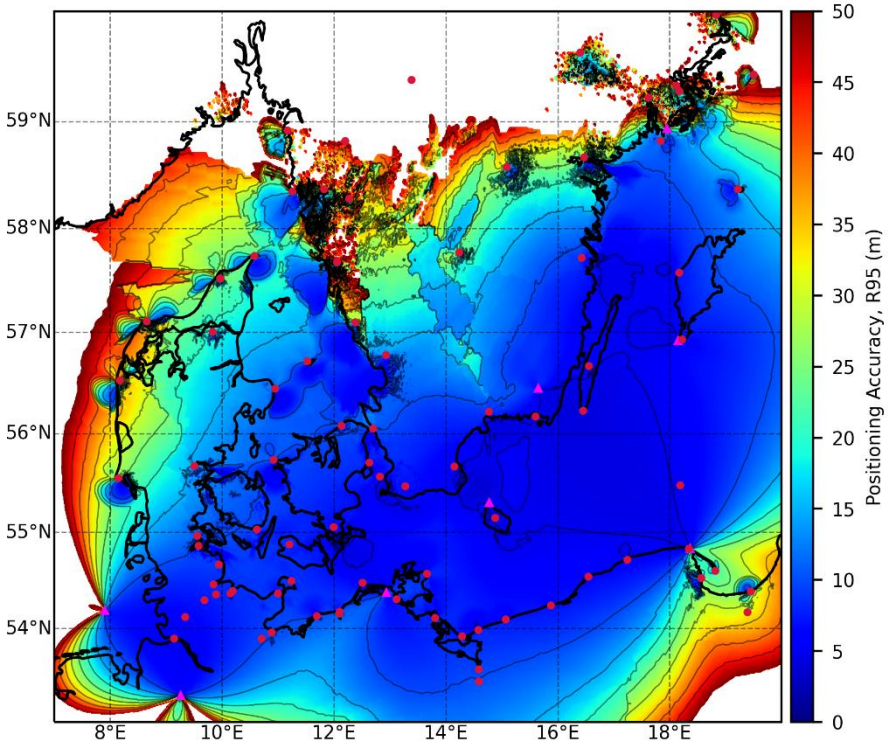

Figure 20: Predicted daytime positioning accuracy for the combined MF/VDES configuration, including the effects of multipath signal propagation (note: the multipath model used has yet to be fully validated); red dots – VDES stations; magenta triangles – MF stations.

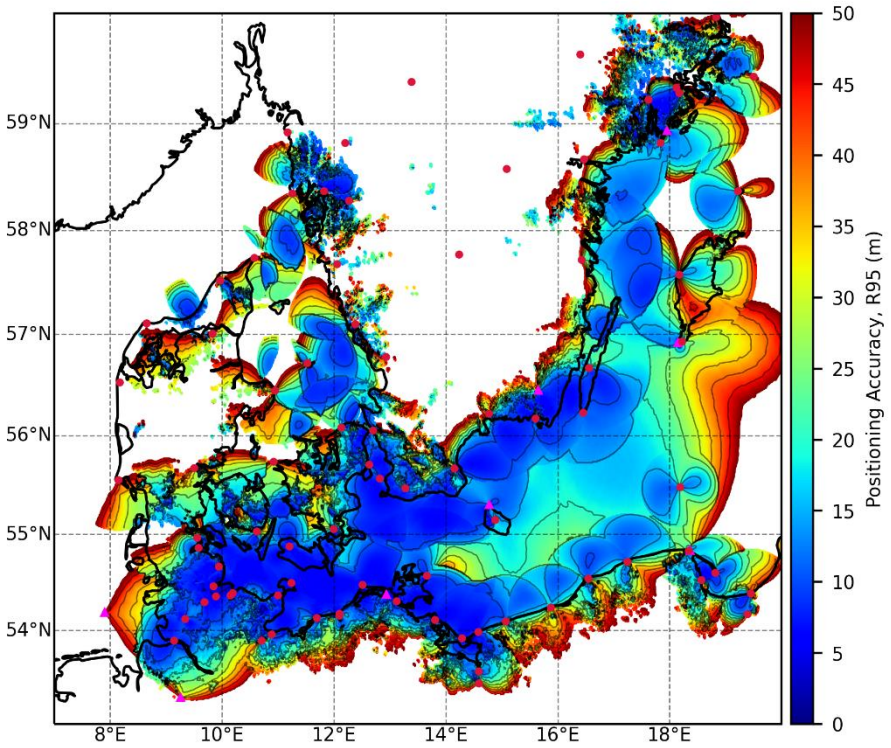

Figure 21: Predicted night-time positioning accuracy for the combined MF/VDES configuration, assuming a multipath-free VDES propagation channel; red dots – VDES stations; magenta triangles – MF stations.

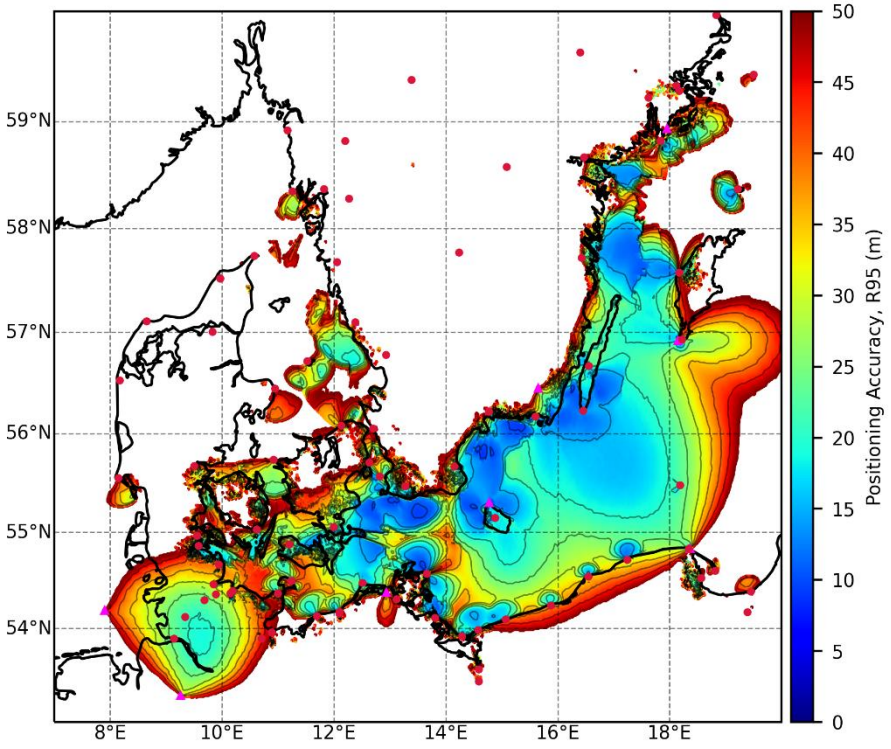

Figure 22: Predicted night-time positioning accuracy for the combined MF/VDES configuration, including the effects of multipath signal propagation (note: the multipath model used has yet to be fully validated); red dots – VDES stations; magenta triangles – MF stations.

5.6 Traceability

Experimental data for combined MF/VDES R-Mode positioning was not available at the time of writing; however, traceability information for the standalone MF and VDES R-Mode models can be found in report [2] and Section 3.8 of this report, respectively.

6 Suggestions for Further Work

Significant improvements in coverage and performance could likely be achieved by relaxing some of the assumptions used in this study, Future work could, for example, consider:

- The use of a positioning algorithm that requires less than four R-Mode stations to be simultaneously in view;
- The use of a more robust modulation and coding scheme (MCS) for the navigation data broadcasts, characterised by a lower C/N_0 threshold; this could include the existing VDE-TER 25 kHz-bandwidth MCS' or a new 100 kHz scheme and would lead to an extended R-Mode station range;
- The feasibility of each R-Mode station broadcasting the navigation data also for its neighbours, making it possible for a receiver to obtain all required navigation data from a single R-Mode station (note that, currently, the receiver is required to be within the "data" coverage area of at least four stations, which greatly reduces the achievable coverage);
- The use of another (other than VDE-TER and MF beacon) data channel for the navigation data delivery, including potentially VDE-SAT.

Note: Further work is required to better characterise and understand the impact of multipath signal propagation and terrain elevation on the achievable ranging performance. The VDES multipath model presented in this report should be considered a first step in this process rather than a definitive answer.

References

[1] M. Hoppe, 'VDES R-Mode Coverage Prediction and Accuracy Estimation', Contract Letter, Jun. 2020.

[2] C. Hargreaves, 'MF R-Mode Coverage Prediction and Accuracy Estimation', GLA R&D (GRAD), Unpublished Technical Report RPT-07-CH-19, v. 0.2, Mar. 2019.

[3] A. Grant, 'GRAD Proposal for Coverage Modelling of VDES R-Mode Transmissions around the Baltic Sea Region, and the Combination of Selected VDES and MF R-Mode Stations.', GLA R&D (GRAD), May 2020.

[4] M. Hoppe, 'List of AIS Stations in the Baltic Region'. Aug. 2020.

[5] ITU, 'A General Purpose Wide-range Terrestrial Propagation Model in the Frequency Range 30 MHz to 50 GHz', Recommendation ITU-R P.2001-3, Aug. 2019. [Online]. Available: https://www.itu.int/dms_pubrec/itu-r/rec/p/R-REC-P.2001-3-201908-I!!PDF-E.pdf.

[6] J. Safar, A. Grant, P. Williams, and N. Ward, 'Performance Bounds for VDES R-mode', *Journal of Navigation*, vol. 73, no. 1, pp. 92–114, Jan. 2020.

[7] IALA, 'GNSS Vulnerability and Mitigation Measures', Recommendation 129, Dec. 2012.

[8] J. Safar, 'Stakeholder Requirements for R-Mode', presented at the IALA Workshop on R-Mode, St-Germain-en-Laye, France, Sep. 2019.

[9] 'Expected Value', *Wikipedia*, Aug. 2020. https://en.wikipedia.org/wiki/Expected_value.

[10] D. Chazan, M. Zakai, and J. Ziv, 'Improved Lower Bounds on Signal Parameter Estimation', *IEEE Transactions on Information Theory*, vol. 21, no. 1, pp. 90–93, Jan. 1975, doi: 10.1109/TIT.1975.1055325.

[11] M. Wirsing, A. Dammann, and R. Raulefs, 'Designing a Ranging Signal for use with VDE R-Mode', in *2020 IEEE/ION Position, Location and Navigation Symposium (PLANS)*, Portland, OR, USA, Apr. 2020, pp. 822–826, doi: 10.1109/PLANS46316.2020.9109855.

[12] NIT, 'AIS and VDES Ranging - Measurements Results', R-Mode Baltic, GA5.3/5/4, Dec. 2019.

[13] A. von Engeln, G. Nedoluha, and J. Teixeira, 'An Analysis of the Frequency and Distribution of Ducting Events in Simulated Radio Occultation Measurements based on ECMWF Fields: DISTRIBUTION OF DUCTING EVENTS', *Journal of Geophysical Research: Atmospheres*, vol. 108, no. D21, Nov. 2003, doi: 10.1029/2002JD003170.

[14] I. Harre, 'A Standardized Algorithm for the Determination of Position Errors by the Example of GPS with and without Selective Availability', *International Hydrographic Review*, vol. 2, no. 1, Jun. 2001.

A VDES Stations Considered

Details of the (potential future) VDES stations considered in this study, as provided by WSV [4], are listed below. Assumptions made by GRAD are highlighted in turquoise.

Country	Station Name	Latitude (° N)	Longitude (° E)	Antenna Height (m above sea level)	TX Power (W)	Antenna Gain (dBi)	TX Feeder Loss (dB)
Germany	Brunsbüttel	53.8901	9.14313	25.5	12.5	8	0.7
Germany	Buk	54.1319	11.6936	93	12.5	8	0.7
Germany	Dänholm	54.3061	13.1184	52.5	12.5	8	0.7
Germany	Darßer Ort	54.4748	12.5043	52.5	12.5	8	0.7
Germany	Eckernförde	54.4596	9.84277	42	12.5	8	0.7
Germany	Friedrichsort	54.3906	10.1898	29	12.5	8	0.7
Germany	Groß Klein	54.1539	12.0926	22	12.5	2.15	0.7
Germany	Grüntal	54.12	9.33306	52	12.5	8	2.7
Germany	Heiligenhafen	54.3662	10.9977	72	12.5	8	0.7
Germany	Holnis	54.8618	9.5735	40	12.5	2.15	0.7
Germany	Kappeln	54.6646	9.93583	45.5	12.5	6.15	0.7
Germany	Karlshagen	54.109	13.8077	79.5	12.5	8	0.7
Germany	Kiel-Wik	54.3642	10.145	68	12.5	8	2.7
Germany	Königsförde	54.3575	9.88306	45	12.5	8	2.7
Germany	Lübeck	53.8943	10.7026	32.5	12.5	2.15	0.7
Germany	Marienleuchte	54.495	11.2382	47	12.5	8	0.7
Germany	Rendsburg	54.2944	9.68222	56.5	12.5	8	2.7
Germany	Stubbenkammer	54.572	13.6581	173.5	12.5	8	0.7
Germany	Travemünde	53.9607	10.8833	19.5	12.5	8	0.7
Germany	Warnemünde	54.1773	12.0977	63.5	12.5	8	0.7
Poland	Elewator Ewa	53.4371	14.5842	64	12.5	5	1.2
Poland	Police	53.5648	14.5856	64	12.5	5	1.2
Poland	Swinoujscie	53.9197	14.2865	43	12.5	5	1.2
Poland	Kikut	53.9814	14.5803	95	12.5	5	1.2
Poland	Niechorze	54.0947	15.0639	65	12.5	5	1.2
Poland	Gaski	54.2429	15.8727	50	12.5	5	1.2
Poland	Jaroslawiec	54.5397	16.5423	51	12.5	5	1.2
Poland	Czolpino	54.7183	17.2413	75	12.5	5	1.2
Poland	Rozewie	54.8304	18.3363	85	12.5	5	1.2
Poland	Hel	54.6	18.8129	33	12.5	4	1.2
Poland	Krynica Morska	54.3854	19.4507	53	12.5	5	1.2
Poland	AIS Baltic Beta	55.4814	18.1827	41	12.5	3.15	1.2
Poland	RL Gdynia	54.5293	18.5596	35	12.5	3.15	1.2
Poland	Elblag	54.1718	19.3879	10	12.5	3.15	1.2
Sweden	Gävle	60.62	17.12	231	12.5	2	3
Sweden	Östhammar	60.25	18.07	303	12.5	2	3
Sweden	Väddö	59.97	18.83	168	12.5	2	3
Sweden	Svenska Högarna	59.43	19.5	47	12.5	2	3
Sweden	Nacka	59.28	18.17	280	12.5	2	3
Sweden	Kaknäs	59.33	18.12	181	12.5	2	3
Sweden	Västerås	59.63	16.4	240	12.5	2	3
Sweden	Södertälje	59.22	17.62	140	12.5	2	3
Sweden	Torö	58.82	17.83	118	12.5	2	3
Sweden	Norrköping	58.67	16.47	283	12.5	2	3
Sweden	Gotska Sandön	58.37	19.22	79	12.5	2	3

Sweden	Visby	57.58	18.17	243	12.5	2	3
Sweden	Hoburgen	56.93	18.22	93	12.5	2	3
Sweden	Västervik	57.72	16.42	325	12.5	2	3
Sweden	Kalmar	56.67	16.55	166	12.5	2	3
Sweden	Ölands Södra Udde	56.23	16.45	127	12.5	2	3
Sweden	Karlskrona	56.17	15.6	92	12.5	2	3
Sweden	Karlshamn	56.22	14.77	222	12.5	2	2.4
Sweden	Kivik	55.67	14.15	239	12.5	2	1.17
Sweden	Trelleborg	55.47	13.27	181	12.5	2	3.9
Sweden	Öresundsbron	55.57	12.82	200	12.5	2	5
Sweden	Helsingborg	56.05	12.7	101	12.5	2	1.2
Sweden	Halmstad	56.78	12.93	419	12.5	2	3
Sweden	Varberg	57.1	12.38	209	12.5	2	3
Sweden	Göteborg	57.68	12.05	256	12.5	2	3
Sweden	Kungshamn	58.35	11.25	110	12.5	2	3
Sweden	Uddevalla	58.37	11.82	342	12.5	2	3
Sweden	Strömstad	58.92	11.17	95	12.5	2	3
Sweden	Trollhättan	58.28	12.27	172	12.5	2	3
Sweden	Bäckefors	58.82	12.2	402	12.5	2	3
Sweden	Karlstad	59.38	13.38	200	12.5	2	3
Sweden	Motala	58.58	15.08	323	12.5	2	3
Sweden	Jönköping	57.77	14.23	379	12.5	2	3
Denmark	Lynetten	55.7067	12.6228	91	12.5	2.15	1.2
Denmark	Vejby	56.0792	12.1294	107	12.5	2.15	1.2
Denmark	Aarsballe	55.1486	14.8806	226	12.5	2.15	1.2
Denmark	Røsnæs	55.7369	10.9203	142	12.5	2.15	1.2
Denmark	Mern	55.0528	11.9894	266	12.5	2.15	1.2
Denmark	Karleby	54.8731	11.1983	148	12.5	2.15	1.2
Denmark	Svendborg	55.0286	10.615	107	12.5	2.15	1.2
Denmark	Felsted	54.9653	9.55417	212	12.5	2.15	1.2
Denmark	Vejle	55.6758	9.50417	219	12.5	2.15	1.2
Denmark	Bovbjerg	56.53	8.16833	111	12.5	2.15	1.2
Denmark	Hanstholm	57.1092	8.65	121	12.5	2.15	1.2
Denmark	Fornæs	56.4475	10.9467	114	12.5	2.15	1.2
Denmark	Anholt	56.7172	11.5203	89	12.5	2.15	1.2
Denmark	Frejlev	57.0042	9.82639	172	12.5	2.15	1.2
Denmark	Hirtshals	57.5242	9.96472	109	12.5	2.15	1.2
Denmark	Læsø	57.5242	9.96472	109	12.5	2.15	1.2
Denmark	Skagen	57.7392	10.5758	90	12.5	2.15	1.2
Denmark	Blåvand	55.5522	8.13972	103	12.5	2.15	1.2

Table 1: VDES stations considered.

B MF Stations Considered

A sub-set of MF radiobeacon stations used in study [2] was selected by WSV for consideration in the present work. The details of the selected stations are provided below.

Country	Station Name	Latitude (° N)	Longitude (° E)
Germany	Zeven	53.284648	9.262353
Germany	Helgoland	54.185986	7.905295
Germany	Groß Mohrdorf	54.374000	12.93445
Poland	Rozewie	54.830622	18.366879
Sweden	Nynashamn	58.933333	17.95000
Sweden	Holmsjö	56.450000	15.65000
Sweden	Hoburg	56.916667	18.15000
Denmark	Hammerodde	55.298167	14.773833

Table 2: MF stations considered.

C CSV File Format

Each comma-separate values (CSV) file produced in this study contains a header row with the following information:

```
Southern latitude, northern latitude, western longitude, eastern longitude, resolution, mask value
```

The first four values in the header are the WGS-84 coordinates of the bounding box for the given data array and are expressed in decimal degrees. North latitude and East longitude are taken as positive.

The fifth value defines the resolution of the latitude/longitude grid for the array, expressed in decimal degrees.

The sixth value identifies a number that is used to mask invalid data points. For the station/system coverage and position error arrays, all data points lying outside the station/system coverage area are marked as invalid. For the ranging error arrays, the mask is applied to the points where the error exceeds a certain threshold.

The following rows then contain the data for all points lying on the latitude/longitude grid defined in the header. Each row represents a particular latitude, with data for different longitudes separated by commas. Latitude and longitude increase with an increasing row and column index, respectively.